RSC Advances

ROYAL SOCIETY OF CHEMISTRY

www.rsc.org/advances

Hematite/N-doped graphene nanohybrids were prepared by an *in situ* simultaneous reduction–doping strategy, exhibiting excellent photocatalytic activity for phenol decomposition.

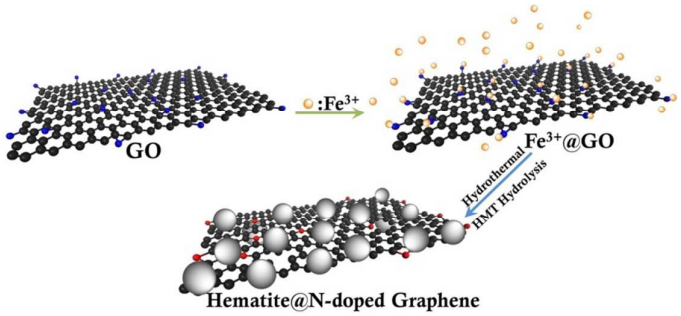

Journal Name

RSCPublishing

COMMUNICATION

In situ simultaneous reduction-doping route to synthesize hematite/N-doped graphene nanohybrids with excellent photoactivity†

Cite this: DOI: 10.1039/x0xx00000x

Yun-Pei Zhu,[a] Tie-Zhen Ren,[b] Yu-Ping Liu[a] and Zhong-Yong Yuan*[a]

Received 00th January 2012,
Accepted 00th January 2012

DOI: 10.1039/x0xx00000x

www.rsc.org/

An in situ simultaneous reduction–doping strategy was carried out based on the hydrolysis of hexamethylenetetramine at evaluated temperature to prepare hematite/N-doped graphene nanohybrids with excellent photocatalytic activity for phenol decomposition under visible light illumination.

As a rising star on the horizon of materials science, graphene has attracted tremendous attention recently due to its remarkable physical and chemical properties, representing a leading candidate in a variety of applications including electronic, optical, and catalytic fields.[1] Classical "top-down" approach to obtain graphene involves chemical exfoliation of graphite or longitudinal "unzipping" of carbon nanotubes.[2] The chemical exfoliation of graphite is considered to be of high efficiency and yields in preparing multi-layered graphene oxide (GO). In addition, abundant oxygen functionalities on the GO surface are of great significance since they provide reactive sites for chemical or post modification. However, contrary to graphene, GO is electronically insulating and has to be reduced into a conductive material. But the most effective chemical reduction routes consist in the exposition of the substrate, additional reduction agents, and/or additional calcination steps.[3] Developing easy and user–friendly strategies to achieve the reduction of GO is an important issue of research, as these approaches would open the way to several applications such as photoelectronics and catalysis.

Currently an attractive challenge is to anchor narrow band gap semiconductors such as hematite (α–Fe_2O_3) on graphene for preparing various nanohybrids, in which graphene is widely recognized to perform as an electron collector and transporter to effectively prohibit electron-hole recombination, thus enhancing the photoelectronic performance.[4] Several methods have been developed to engineer α–Fe_2O_3/graphene nanostrcutures,[5] showing favorable photocatalytic activity due to the fast transfer of photo-generated electrons from α–Fe_2O_3 to graphene sheets. However, previously reported solution-based approaches for producing nanocomposites between graphene and α–Fe_2O_3 nanoparticles generally involve multiple steps to achieve architectural control and heterostructure. Also, the need of binding agents or surfactants could occlude internal interfaces and likely compromise ultimate catalytic performance.[6] Moreover, heteroatom doping such as nitrogen into graphene sheets will be the key to the future applications because doping can tailor the electronic and chemical properties of graphene, thereby modulating the electronic and catalytic performances.[7] Nonetheless, it remains a challenge to prepare N–doped graphene and α–Fe_2O_3 nanocomposites through a facile method.

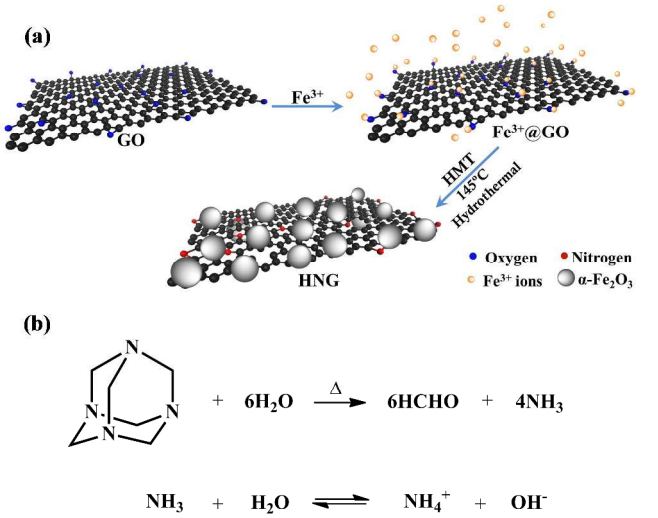

Scheme 1 Schematic illustration of the formation mechanism of the HNG nanohybrid.

In this communication, we report a novel in situ simultaneous reduction-doping (SRD) route for preparation of hematite/N-doped graphene nanohybrids (HNG) with excellent photocatalytic

activity and stability. As illustrated in Scheme 1, GO contains various reactive oxygen functionalities on the sheet surface including hydroxyl and epoxy groups on the basal plane and smaller amounts of carboxy, carbonyl, phenol, lactone and quinone at the sheet edges, making GO a possible precursor for immobilization of metal ions. After addition of $FeCl_3$ into the GO suspension, Fe^{3+} ions were coordinated by oxygenous groups on GO, where GO served as the anchoring sites for α–Fe_2O_3 nanoparticles. The present SRD methodology is dependent on the hydrolysis of hexamethylenetetramine (HMT) into formaldehyde and ammonia at elevated temperature.[8] Ammonia was considered as nitrogen source for doping[9] and pH buffer for the growth of α–Fe_2O_3. The synchronous reduction and nitrogen doping of GO into N-doped graphene (NG) by formaldehyde and ammonia, and the formation of hematite through the hydrolysis of Fe^{3+}, subsequently in situ loading onto graphene through chemical bonds (Fe–O–C) could be realized to result in HNG. The dispersion of hematite could inhibit the collapse and restacking of exfoliated sheets of graphene during reduction process.

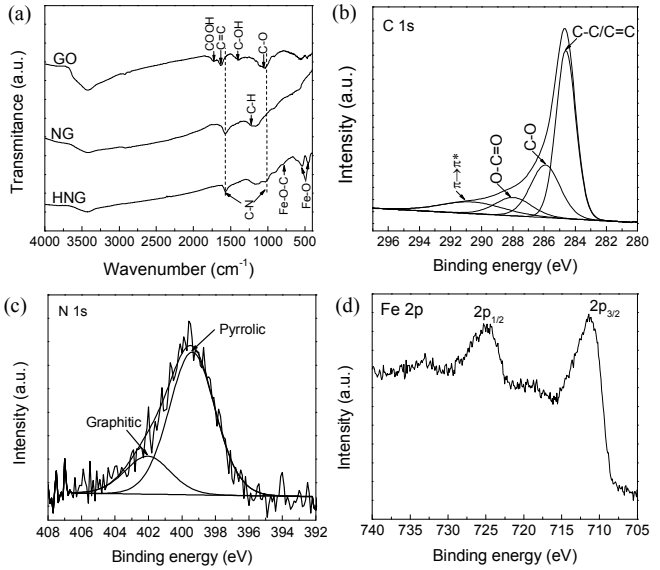

Fig. 1 (a) FT-IR spectrum of GO, NG, and HNG; High-resolution XPS spectrum of C 1s (b), N 1s (c), and Fe 2p (d) for HNG.

The colour of the GO suspension altered from golden-brown to black after hydrothermal treatment (Fig. S1, ESI), revealing that the reduction of GO occurred. In the FT–IR spectrum of HNG and NG (Fig. 1a), the characteristic bands of GO (1734 cm^{-1} for C=O stretching, 1395 cm^{-1} for C–OH, and 1061 cm^{-1} for C–O stretching) are vanished or weakened, manifesting that GO was reduced to graphene. Noticeably, a shoulder band at 798 cm^{-1} assigned to Fe–O–C can be observed.[10] This suggests that Fe atoms in Fe_2O_3 can intimately interact with the graphene matrix to form chemisorption interfaces through Fe–O–C bonding. The existence of Fe–O–C linkages would favour the charge transfer between hematite and graphene upon light excitation. Furthermore, new peaks are identified at 1020 and 1569 cm^{-1} in the case of NG and HNG, which can be ascribed to sp^2 bonded C–N.[11] The XPS spectra of the C 1s core level for HNG in Fig. 1b can be deconvoluted into four components including the sp^2 carbon (284.6 eV), C–N (285.9 eV)], C=O (287.9 eV), and $\pi \rightarrow \pi^*$ (291.2 eV).[12] The significant drops of the peak 287.9 eV implies the successful reduction of GO after the hydrothermal process. The deconvolution of N 1s spectrum indicates the presence of pyrrolic N (399.5 eV) and graphitic N (401.9 eV).[13] The two major components at binding energies of 711.3 and 724.8 eV accompanied with two satellites are attributed to $2p_{3/2}$ and $2p_{1/2}$ core levels for α–Fe_2O_3.[14] The atomic ratio of the synthesized HNG based on XPS characterization were obtained to be 0.044 and 0.203 for Fe/C and O/C, respectively.

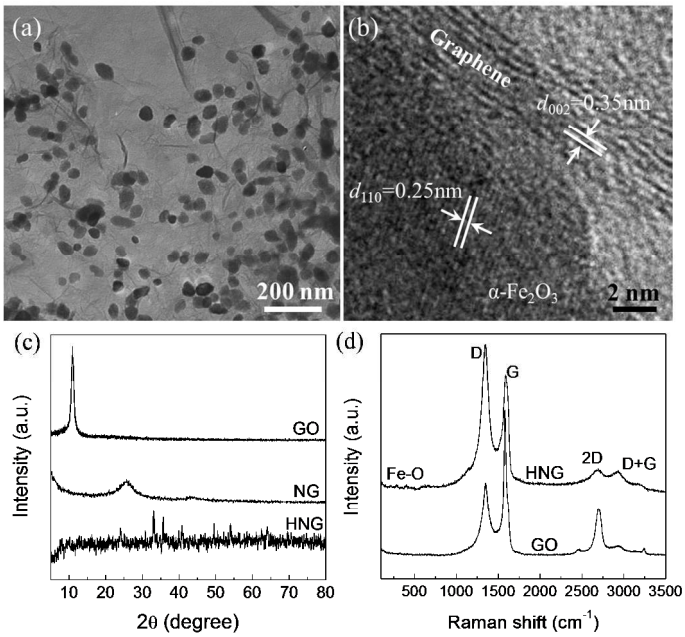

Fig. 2 (a,b) TEM images of HNG; (c) XRD patterns of GO, NG and HNG; (d) Raman spectra of GO and HNG.

TEM characterization was taken into illustrate the microstructures of the hybrid (Fig. 2a, ESI). The hematite nanoparticles (15–40 nm) in the hybrid are homogeneously dispersed on the N-doped graphene sheets. In contrast, hematite nanoparticles prepared via the same method but without GO aggregated severely (Fig. S2a). NG showed a crumpled sheet-like morphology, demonstrating no obvious change in comparison with GO (Fig. S3, ESI). The regularity and fine dispersion of α-Fe_2O_3 nanoparticle on graphene is greatly beneficial for the photocatalytic process. According to N_2 sorption analysis (Fig. S4, ESI), the multi-point BET surface area HNG was determined to be 125 m^2 g^{-1}, which is higher than those of hematite nanoparticles (83 m^2 g^{-1}) and NG (108 m^2 g^{-1}). This indicates that the hematite nanoparticles could perform as spacers to create porous architecture between the graphene sheets, which would thus facilitate mass transfer across the hybrid. To shed light on the interface structure between the two phases, the hybrid was further examined with high–magnification TEM (Fig. 2b). It can be clearly seen that graphene nanosheets

with the basal plane tightly linked with hematite nanoparticles. A crystalline nanoparticle with an interplanar spacing of 0.25 nm can be attributed to (110) plane of rhombohedral hematite. The graphene layers are interrupted, curved and have plentiful defects. The interlayer separation of the graphene substrate estimated from the HRTEM is 0.35 nm. The XRD pattern of NG (Fig. 2c) displays a broad diffraction at 2θ = 25.6°. This can be attributed to a layer–to–layer distance of (002) of about 0.35 nm of graphene, coinciding with the TEM observation. A series of diffraction peaks for HNG can be indexed to rhombohedral phase α–Fe_2O_3 (JCPDS no. 84–0311).

Raman spectroscopy is an effective way to investigate the electronic and phonon structures in pristine and doped carbon-based materials (Fig. 2d). Signals of the Fe–O band (292 and 412 cm^{-1}) from hematite,[15] and the D band (1344 cm^{-1}), G band (1590 cm^{-1}), 2D band (2686 cm^{-1}) and combination of D + G band (2927 cm^{-1}) from graphene[5c] can be observed in HNG, confirming the formation of composite of graphene and hematite. The increased I_D/I_G ratio of HNG (1.53) in comparison with GO (0.85) can be resulted from the existence of abundant structure defects. The shift of the G band for HNG composite by 16 cm^{-1} as compared to that of GO signifies the strong interaction between graphene and hematite,[16] which is consistent with the FT–IR and TEM characterization. On the other side, the shape and position of the overtone of the 2D band are a significant fingerprint which can be related to the formation and the layer numbers of graphene sheets.[17] The 2D band of HNG appears as a wider and nearly asymmetrical peak with a little shift to larger wavenumbers as compared to GO, indicating the multilayer characteristics for the HNG sample.[17]

In this work, HMT played a triple role of reducing agent, nitrogen donor, and pH controller in the hydrothermal system. The thermal decomposition of HMT provided the consecutive supply of formaldehyde and ammonia, leading to the reduction of GO accompanied with the nitrogen incorporation and the formation of hematite nanoparticles on the graphene nanosheets. Moreover, by simply adjusting HMT/$FeCl_3$ ratio, magnetite/NG nanohybrid could be obtained (Fig. S2b and S5, ESI), wherein the superfluously formed formaldehyde could partially reduce Fe^{3+} to Fe^{2+} as well. It is noteworthy that the resultant magnetism (Fig. S6, ESI) shows potential in the field of separation and biomaterials. We expect that this SRD methodology could be extended to prepare other N–doped graphene–based composites hybridized with oxides and even hydroxides like MnO_2/NG, Co_3O_4/NG, and $Ni(OH)_2$/NG.

To prove the influence of the incorporated graphene on the favourable separation and transportation of photo-generated carriers under visible light illumination, photocurrent measurements were carried out on the synthesized catalysts after deposition on transparent conductive glasses. As shown in Fig. S7a, the fast and stable photocurrent response of the HNG electrode for each switch–on and switch–off light cycles can be observed and the photoresponsive phenomenon is entirely reproducible. With stopping of the irradiation, the photocurrent decreases to zero instantly. In contrast, the NG modified electrode shows almost no photoelectrochemical effect, and the α-Fe_2O_3 electrode produces a weaker photocurrent density (8.93 μA cm^{-2}) in comparison with that of HNG (25.6 μA cm^{-2}). In addition, photocurrent-potential curves (Fig. S7b, ESI) under light excitation of the α-Fe_2O_3 and HNG electrodes exhibit that both generate anodic current with applied bias. However, under the same conditions, HNG presents a photocurrent of 1.94 mA cm^{-2}, which is about 2 times higher than α-Fe_2O_3 (0.79 mA cm^{-2}). This means that a higher number of electrons are generated from the HNG electrode, resulting in larger photocurrent density. The improvement of photocurrent reveals that the photo-induced electrons in the well allocated hematite nanoparticles could be transferred into graphene and then percolate to the collecting electrode.[16,18] Since the graphene nanosheet possessed extensively conjugated sp^2–hybridized network, it presents high conductivity and also performs as election sink. This remarkable property of graphene makes it advantageous for transferring the photoinduced electrons from hematite and suppressing the recombination of charge carriers via channelizing the photogenerated electrons through its surface, which played an indispensable role in enhancing the photocurrent. Moreover, good dispersion and intimate attachment of hematite nanoparticles over the graphene nanosheets were responsible for utilizing electrons that arised from α–Fe_2O_3 during the photochemical process. These factors are expected to minimize the charge recombination losses, creating a platform in optimizing the photocatalytic performance.

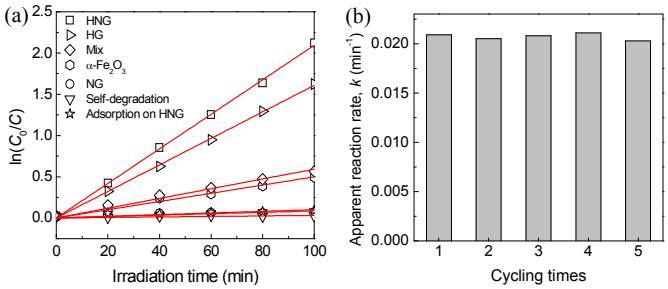

Fig. 3 (a) The photocatalytic activity for phenol degradation under visible light irradiation for the synthesized catalysts, the red lines in the figure show the fitting results using pseudo-first-order reaction kinetics; (b) reusability of the HNG catalyst for phenol degradation.

A non–self–sensitizing pollutant, phenol, was selected as the probe molecule to evaluate the photocatalytic activity of the synthesized catalysts. The photocatalytic degradation reaction can be assumed to follow a pseudo–first–order expression: $\ln(C_0/C) = kt$, where C_0/C is the normalized concentration and k is the apparent reaction rate (min^{-1}).[19] Fig. 3 shows that the consumption of phenol by the adsorption process in the presence of HNG can be ignored. The decomposition of phenol is negligible under visible light irradiation in the absence of any catalyst or in the presence of NG. However, the photocatalytic activity of HNG (0.0209 min^{-1}) is much higher than that of α–Fe_2O_3 (0.00499 min^{-1}). This can be mainly attributed to the well-defined porosity and intimately anchored hematite nanoparticles on the graphene for the HNG hybrid. Physical mixture of NG and α–Fe_2O_3 (denoted as Mix), in relatively weak contact, shows a

slightly higher reaction rate (0.00592 min^{-1}) than pure α–Fe_2O_3, but not as much as HNG did, suggesting that the intimate contact between graphene and α–Fe_2O_3 is of great significance for the efficient transfer of photo-generated carriers. For comparison, hematite/non–doped graphene (labelled as HG) composite was prepared (see Experimental Section, ESI) and the corresponding photoactivity was tested. Nevertheless, it is found that the reactivity for the HG sample (0.0161 min^{-1}) is inferior as compared to the HNG counterpart, which may be due to that the nitrogen doping can considerably improve the conductivity of graphene (Fig. S8, ESI).[20] Remarkably, the photocatalytic decomposition of phenol on HNG proceeds without noticeable decrease in the activity after five recycles (Fig. 3b), indicating that the synthesized HNG catalyst has an excellent stability and great application potential. The considerable stability of the resultant nanohybrid is quite different from the previous semiconductor-graphene-based composite,[21] implying that the efficient separation of photo-induced carriers contributed to decompose phenol molecules. Notably, in comparison with the photocatalytic reduction processes on the basis of photo-excitation of some semiconductor oxides while using ethanol as hole scavenger,[22] the SRD strategy could achieve a higher reduction degree of GO (about 85%). The existence of a small amount of carbonyl groups reveals they would evade the mild reduction conditions,[23] contributing to the intimate bond between graphene and hematite nanoparticles and the improvement of catalytic activity and stability. The Fe/C/O atomic ratio of the synthesized HNG based on XPS characterization is calculated to be 0.044:0.203:1, showing little change (0.042:0.209:1) even after five times cycling tests. This further suggests the stability of the present graphene-based composite photocatalyst.

In summary, a novel and facile in situ strategy has been taken out to prepare N–doped graphene homogeneously hybridized with hematite nanoparticles depending on the hydrolysis of hexamethylenetetramine into formaldehyde and ammonia under hydrothermal conditions. The good dispersion and attachment of hematite nanoparticles over the graphene endow the resultant nanohybrids with considerably excellent photoactivity and stability for phenol degradation under visible light illumination, due to the inhibited charge recombination losses. Thus this in situ methodology provides an ingenious way to prepare N–doped graphene-based composites hybridized with oxides and even hydroxides, which can further find use in the areas of electrochemical catalytic reactions and supercapacitors.

Acknowledgements

This work was supported by the National Natural Science Foundation of China (21076056 and 21073099), the Specialized Research Fund for the Doctoral Program of Higher Education (20110031110016), the MOE Innovative Team (IRT13022), the 111 project (B12015), and the Key Laboratory of Advanced Catalytic Materials in Zhejiang Normal University (ZJHX201301), and the Ph.D. Candidate Research Innovation Fund of Nankai University.

Notes and references

[a] Key Laboratory of Advanced Energy Materials Chemistry (Ministry of Education), Collaborative Innovation Center of Chemical Science and Engineering (Tianjin), College of Chemistry, Nankai University, Tianjin 300071, China. E-mail: zyyuan@nankai.edu.cn.
[b] School of Chemical Engineering and Technology, Hebei University of Technology, Tianjin 300130, China.
† Electronic supplementary information (ESI) available: Experimental section and detailed characterization. See DOI: 10.1039/x0xx00000x

1 I. V. Lightcap and P. V. Kamat, *Acc. Chem. Res.*, 2013, **46**, 2235.
2 (a) S. Park and R. S. Ruoff, *Nat. Nanotechnol.*, 2009, **4**, 217; (b) V. K. Dmitry, L. H. Amanda, S. Alexander, R. L. Jay, D. Ayrat, B. K. Price and M. T. James, *Nature*, 2009, **458**, 872.
3 (a) J. Z. Wang, C. Zhong, D. Wexler, N. H. Idris, Z. X. Wang, L. Q. Chen and H. K. Liu, *Chem. Eur. J.*, 2011, **17**, 661; (b) B. J. Li, H. Q. Cao, J. Shao, M. Z. Qu and J. H. Warner, *J. Mater. Chem.*, 2011, **21**, 5069; (c) G. M. Zhou, D. W. Wang, F. Li, L. L. Zhang, N. Li, Z. S. Wu, L. Wen, G. Q. Lu and H. M. Cheng, *Chem. Mater.*, 2010, **22**, 5306.
4 Q. J. Xiang, J. G. Yu and M. Jaroniec, *Chem. Soc. Rev.*, 2012, **41**, 782.
5 (a) F. K. Meng, J. T. Li, S. K. Cushing, J. Bright, M. J. Zhi, J. D. Rowley, Z. L. Hong, A. Manivannan, A. D. Bristow and N. Q. Wu, *ACS Catal.*, 2013, **3**, 746; (b) Y. Hou; F. Zuo, A. Dagg and P. Feng, *Nano Lett.*, 2012, **12**, 6464; (c) L. He, L. Jing, Z. Li, W. Sun and C. Liu, *RSC Adv.*, 2013, **3**, 7438; (d) S. Guo, G. K. Zhang, Y. D. Guo and J. C. Yu, *Carbon*, 2013, **60**, 437; (e) L. He, L. Jing, Y. Luan, L. Wang and H. Fu, *ACS Catal.*, 2014, **4**, 990.
6 J. E. Johns, J. M. P. Alaboson, S. Patwardhan, C. R. Ryder, G. C. Schatz and M. C. Hersam, *J. Am. Chem. Soc.*, 2013, **135**, 18121.
7 (a) H. M. Jeong, J. W. Lee, W. H. Shin, Y. J. Choi, H. J. Shin, J. K. Kang and J. W. Choi, *Nano Lett.*, 2011, **11**, 2472; (b) X. R. Wang, X. B. Li, L. Zhang, Y. K. Yoon, P. K. Weber, H. L. Wang, J. Guo and H. J. Dai, *Science*, 2009, **324**, 768; (c) Y. F. Lu, S. T. Lo, J. C. Lin, W. J. Zhang, J. Y. Lu, F. H. Liu, C. M. Tseng, Y. H. Lee, C. T. Liang and L. J. Li, *ACS Nano*, 2013, **7**, 6522.
8 L. Liu, Q. F. Deng, X. X. Hou and Z. Y. Yuan, *J. Mater. Chem.*, 2012, **22**, 15540.
9 S. Chen, J. J. Duan, M. Jaroniec and S. Z. Qiao, *Angew. Chem., Int. Ed.*, 2013, **52**, 13567.
10 H. Zhang, X. J. Lv, Y. M. Li, Y. Wang and J. H. Li , *ACS Nano*, 2009, **4**, 380.
11 (a) X. X. Yang, L. Liu, M. H. Wu, W. L. Wang, X. D. Baiand and E. G. Wang, *J. Am. Chem. Soc.*, 2011, **133**, 13216; (b) P. Wu, Y. D. Qian, P. Du, H. Zhang and C. X. Cai, *J. Mater. Chem.*, 2012, **22**, 6402.
12 (a) B. J. Li and H. Q. Cao, *J. Mater. Chem.*, 2011, **21**, 3346; (b) A. Esfandiar, O. Akhavan and A. Irajizad, *J. Mater. Chem.*, 2011, **21**, 10907; (c) D. Wei, Y. Liu, Y. Wang, H. Zhang, L. Huang and G. Yu, *Nano Lett.*, 2009, **9**, 1752; (d) H. Zhang, T. Kuila, N. H. Kim, D. S. Yu and J. H. Lee, *Carbon*, 2014, **69**, 66.
13 Z. H. Sheng, L. Shao, J. J. Chen, W. J. Bao, F. B. Wang and X. H. Xia, *ACS Nano*, 2011, **5**, 4350.
14 C. J. Jia, L. D. Sun, F. Luo, X. D. Han, L. J. Heyderman, Z. G. Yan, C. H. Yan, K. Zheng, Z. Zhang, M. Takano, N. Hayashi, M. Eltschka, M. Kläui, U. Rüdiger, T. Kasama, L. Cervera-Gontard, R. E. Dunin-Borkowski, G. Tzvetkov and J. Raabe, *J. Am. Chem. Soc.*, 2008, **130**, 16968.

15 R. L. Spray and K. S. Choi, *Chem. Mater.*, 2009, **21**, 3701.
16 G. K. Pradhan, D. K. Padhi and K. M. Parida, *ACS Appl. Mater. Interfaces*, 2013, **5**, 9101.
17 (a) O. Akhavan and E. Ghaderi, *Small*, 2013, **9**, 3593; (b) A. C. Ferrari, J. C. Meyer, V. Scardaci, C. Casiraghi, M. Lazzeri, F. Mauri, S. Piscanec, D. Jiang, K. S. Novoselov, S. Roth and A. K. Geim, *Phys. Rev. Lett.*, 2006, **97**, 187401; (c) I. Calizo, A. A. Balandin, W. Bao, F. Miao and C. N. Lau, *Nano Lett.*, 2007, 7, 2645.
18 W. G. Tu, Y. Zhou, Q. Liu, S. C. Yan, S. S. Bao, X. Y. Wang, M. Xiao and Z. G. Zou, *Adv. Funct. Mater.*, 2013, **23**, 1743.
19 K. Rusevova, R. Köferstein, M. Rosell, H. H. Richnow, F. D. Kopinke and A. Georgi, *Chem. Eng. J.*, 2014, **239**, 322.
20 (a) L. Jia, D. H. Wang, Y. X. Huang, A. W. Xu and H. Q. Yu, *J. Phys. Chem. C*, 2011, **115**, 11466; (b) X. L. Li, H. L. Wang, J. T. Robinson, H. Sanchez, G. DianKov and H. J. Dai, *J. Am. Chem. Soc.*, 2009, **131**, 15939.
21 (a) O. Akhavan, *ACS Nano*, 2010, **4**, 4174; (b) O. Akhavan, M. Abdolahad, A. Esfandiar and M. Mohatashamifar, *J. Phys. Chem. C*, 2010, **114**, 12955.
22 (a) G. Williams, B. Seger and P. V. Kamat, *ACS Nano*, 2008, **2**, 1487; (b) O. Akhavan, *Carbon*, 2011, **49,** 11; (c) G. Williams and P. V. Kamat, *Langmuir*, 2009, **25**, 13869; (d) O. Akhavan and E. Ghaderi, *J. Phys. Chem. C*, 2009, **113**, 20214; (e) O. Akhavan, M. Choobtashani, and E. Ghaderi, *J. Phys. Chem. C*, 2012, **116**, 9653.
23 D. Li, M. B. Muller, S. Gilje, R. B. Kaner and C. G. Wallace, *Nat. Nanotechnol.*, 2008, **3**, 101.